HNPS Advances in Nuclear Physics

Vol 28 (2021)

HNPS2021

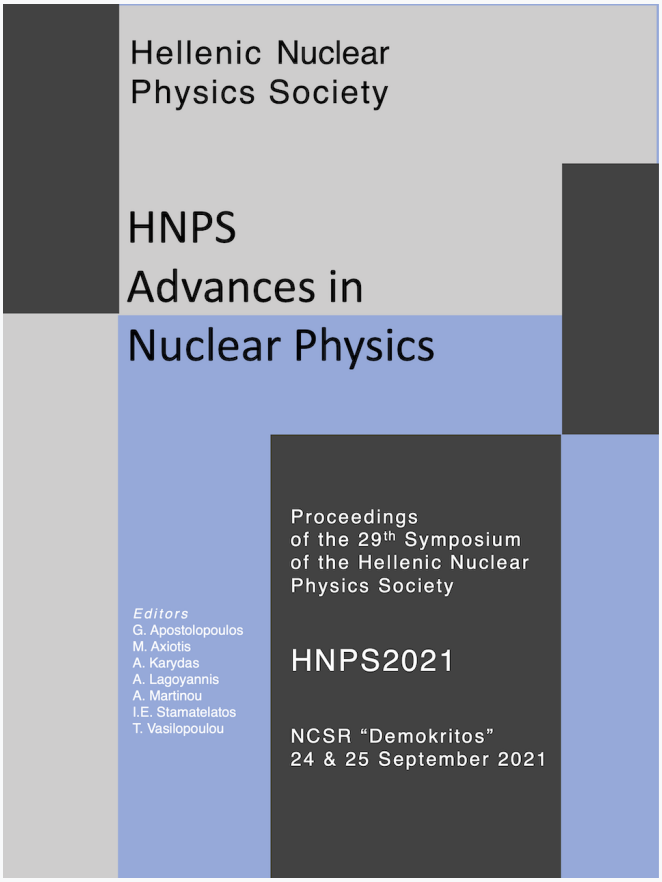

Impact of nuclear mass measurements in the vicinity of 132Sn on the r-process nucleosynthesis

STYLIANOS NIKAS, Anu Kankainen, Olga Beliuskina, Dmitrii Nesterenko

doi: 10.12681/hnps.3605

To cite this article:

NIKAS, S., Kankainen, A., Beliuskina, O., & Nesterenko, D. (2022). Impact of nuclear mass measurements in the vicinity of 132Sn on the r-process nucleosynthesis. *HNPS Advances in Nuclear Physics*, *28*, 86–92. https://doi.org/10.12681/hnps.3605

Impact of nuclear mass measurements in the vicinity of ^{132}Sn on the r-process nucleosynthesis

Stylianos Nikas[1], Anu Kankainen[1], Olga Beliuskina[1], Dmitrii Nesterenko[1], and the IGISOL group[1]

[1]*University of Jyväskylä, P.O. Box 35 (YFL), FI-40014 University of Jyvaskyla, Finland*

Abstract Nuclear masses are a key aspect in the modelling of nuclear reaction rates for the r-process nucleosynthesis. High precission mass measurements drastically reduce the associated uncertainties in the modelling of r-process nucleosynthesis. We investigate the impact of nuclear mass uncertainties on neutron-capture rates calculations using a Hauser – Feshbach statistical code in the vicinity of ^{132}Sn. Finally, we study the impact of the propagated neutron-capture reaction rates uncertainties on the r-process nucleosynthesis. We find that mass measurements with uncertainties higher than 20 keV affect the calculation of reaction rates. We also note that modelling of reaction rates can differ for more than a factor of two even for experimentally known nuclear masses.

Keywords r-process, Penning traps, Hauser-Feshbach, neutron-capture rates

INTRODUCTION

The site of the creation of many heavy elements is a long-lasting question in nuclear astrophysics. Most of the heavy elements are created by two processes, the rapid neutron capture nucleosynthesis (r-process) and the slow neutron capture process (s-process). The r-process is responsible for approximately half of the elemental abundances heavier than Fe in the solar system [1,2]. The r-process is a primary process, which means that it creates both the seeds and the neutrons needed for its operation [2,3]. It is characterized by a series of consecutive neutron captures (n, γ), that lead material away from the valley of stability. These consecutive neutron captures come to a stall when photodisintegrations (γ, n) become comparable to (n, γ) creating a 'waiting point' where material accumulates until β-decay moves material to a higher *Z* number. The r-process abundance pattern is characterized by a three-peak structure, with peaks located at mass numbers A~82,130,195. These peaks are the result of material accumulating in the vicinity of the closed neutron shells due to the slower neutron-capture reaction rates and the longer beta-decay half-lives, which lead to a bending of the path of the r-process close to magic shells. Fission cycling can contribute to the abundances of A~130. Depending on the astrophysical scenario, sufficient large neutron flux can allow the r-process to extend up to the neutron drip line, or in the case of lower neutron fluxes, the r-process to operate closer to stability. The relevant quantity is the neutron to seed ratio, which depends on the electron fraction (Y_e) and the entropy (S) of the astrophysical site we study [2,4].

From the above, it becomes apparent that in order to successfully model the r-process, data for the astrophysical environment (such as the electron fraction (Y_e) expansion timescales and the entropy (S) of the system) as well as nuclear data of the nuclei participating in the r-process (reaction rates, beta-decay rates, fission yields) are requiered [5–7]. Observations of the solar system abundances and metal-poor halo stars indicate at least two different sites where the r-process nucleosynthesis operates [3, 8], however, the exact astrophysical conditions under which the r-process operates remain a mystery to today. The only direct observation about the site of the r-process points to neutron-star mergers [9–14], but other sites like supernovae or magnetohydrodynamical jet supernovae cannot be excluded. The lack of measurements of the properties of nuclei that participate in the r-process are further complicating this endeavor.

The solar abundance pattern is the only data available for comparison and evaluation of the r-process modelling. The r-process abundances are the residual of the solar abundances after we subtract s-process abundances. Any uncertainties associated with the r-process abundances are due to the uncertainty of the contribution of the s-process to the total solar abundance (Fig. 1). Therefore, the study of the r-process is inherently an inverse problem where the output is known and the input must be determined [15]. For such problems sensitivity studies, following Monte Carlo methods, as well as reverse engineering of relevant quantities can be employed. Thus, reducing the uncertainties from the nuclear side could help determine the exact astrophysical conditions under which the r-process operates and visa-versa. However, the measurement of low-energy neutron-capture cross sections is experimentally a very challenging task. Hence, we must rely on nuclear modelling. More specifically to model the reaction rates for the elements participating in the r-process we deploy the Hauser-Feshbach statistical model. It allows us to model reaction rates using experimental data such as nuclear masses, and statistical quantities like nuclear level densities and gamma strength functions.

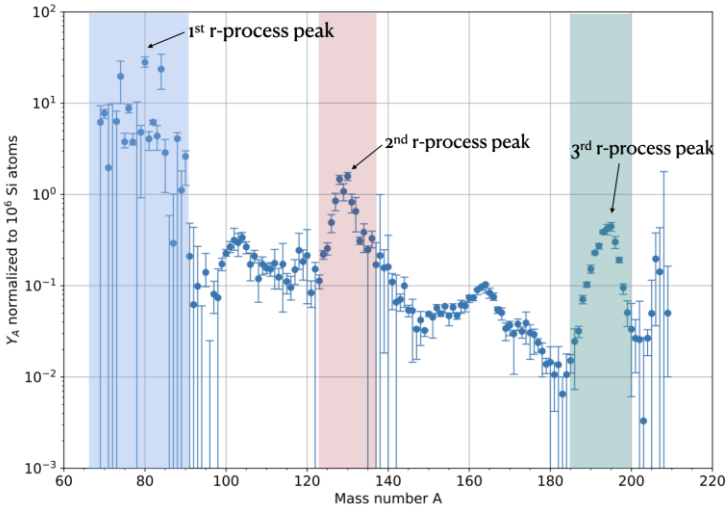

Fig. 1: *Solar system r-process abundances as a function of mass number A we clearly see the three abundance peaks at A~82,130,190 labelled with blue, red, and green colors. Data taken from [16].*

Although the modelling of reaction rates is consistent for known nuclear masses and close to stability, as we move away from stability calculated reaction rates can differ by orders of magnitude [5-6, 17–20]. Large uncertainties in nuclear masses, as well as the divergence of theoretical models used for the statistical quantities, and the unknown nuclear masses drastically affect reaction rates calculations. New radioactive beam facilities, such as FRIB and FAIR, can give a solution to this problem by giving access to measure properties of exotic nuclei that previously were out of our reach. Until these facilities come online, the quest to accurately measure the properties of the current accessible nuclei are ongoing and fruitful. New experimental techniques and the commission of high precision measurement equipment, such as the JYFLTRAP Penning trap in the JYFL Accelerator Laboratory [21] and multi-reflection time of flight techniques at TITAN [22] can drastically reduce the uncertainties in nuclear mass measurements [20, 23] allowing for better modelling of the relevant for the r-process quantities.

In this study we focus on elements in the vicinity of the 2nd r-process peak (Fig. 1). This peak is associated with the main r-process and can be created for a wide range of conditions. Since the astrophysical scenarios behind the creation of the second peak are so broad, we will mainly focus on the impact nuclear mass uncertainties have on the modelling of nuclear reaction rates and discuss the

impact on the r-process on a follow-up paper. More specifically we will focus on the calculation of neutron-capture rates for a range of known masses with Z=40-60. We will evaluate the impact of nuclear mass uncertainties on the calculated reaction rates and make an estimation of how precision mass measurements using Penning traps can reduce the associated errors.

AVAILABLE NUCLEAR MASSES IN THE VICINITY OF THE 2ND R-PROCESS PEAK

Nuclei close to doubly magic ^{132}Sn are important for nuclear structure and the r-process. Mass measurements in this region provide information on the evolution of the Z=50 and N=82 shell closures, one- and two-neutron separation energies and pairing effects in the region. Recent experimental efforts to measure masses have yielded a handful of new mass values over the last few years. In Fig. 2 we compare experimental mass values from the Atomic Mass Evaluation 2016 (AME16) [23] and 2020 (AME20) [24]. From this plot we observe that while there is only one new mass measurement (^{132} Cd) in the vicinity of N=82, new mass measurements reported in AME20 have differences up to 0.5 MeV compared to AME16. New measurements often correct previously reported mass values. In Fig. 3 we show the 1σ error in the mass excess values of AME20. We also circle nuclei with large uncertainties that can be measured with Penning-traps, thus drastically increasing the accuracy of the mass value. The biggest limitation of Penning-trap measurements is the lifetime of the nucleus. Typically, lifetimes larger than 100 ms can be measured using Penning traps. Recently, several mass measurements of neutron-rich nuclei have been performed with JYFLTRAP, see e.g., [26].

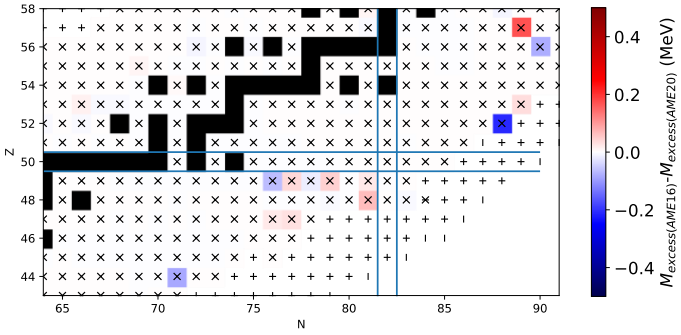

Fig. 2: *In this figure we compare in a color-coded neutron vs proton number plane (N-Z plane) the differences in measurements of mass-excess values reported in AME16 and AME20. With black we label stable nuclei. In addition, we label with (x) measured masses in AME20, with (+) extrapolated masses which are both in AME16 and AME20 and with (|) extrapolated masses that are reported only in AME20. Vertical and horizontal lines label the N=82 closed neutron and Z=50 proton shell respectively*

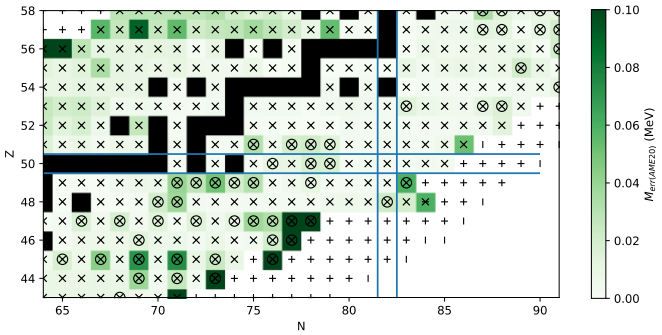

Fig. 3: *In this figure we plot in a color-coded neutron vs proton number plane (N-Z plane) the 1 σ error of the mass-excess values reported in AME20. With black we label stable nuclei. In addition, we label with (x) measured masses in AME20, with (+) extrapolated masses which are both in AME16 and AME20 and with (|) extrapolated masses that are reported only in AME20. We circle the elements that are accessible for Penning traps and for which the mass measurements can drastically reduce the error bar. Vertical and horizontal lines label the N=82 closed neutron and Z=50 proton shell respectively.*

THE HAUSER FESHBACH STATISTICAL MODEL – MASS DEPENDENCIES

To model reaction rates, we use the Hauser-Feshbach statistical code TALYS [26]. The statistical model predicts reaction cross sections averaged over many resonances in the intermediate nuclei.
If we sum all the possible angular momentum states *l*, we can write the absorption cross section that corresponds to all non-elastic channels [27] as:

$$\sigma = \frac{\pi}{k^2}\sum_{l=0}^{\infty}(2l+1)T_l \tag{1}$$

where T_l is the transmission coefficient for the incoming particle, $k = \frac{\sqrt{2\backslash muE}}{\hbar}$ is the wave number and μ the reduced mass of the projectile target system. *Eq. 2* describes the cross-section for the formation of the compound system on an excited state. The compound system will be created at an excited state with energy *Q+E*, where *Q* is the *Q-value* and *E* is the center of mass energy of the projectile. We can use Eq. (1) to estimate neutron-capture cross sections. In this case we do not require the projectile to overcome the Coulomb barrier and thus we can assume the transmission coefficient for direct s-wave ($l = 0$):

$$\sigma \approx \frac{\hbar^2\pi}{2\mu E}T_{l=0} \tag{2}$$

This excited compound nucleus can then de-excite by emitting a particle or a *γ-ray*. This is a clear dependence of reaction-rate calculations with the statistical model on nuclear masses since the mass of a nucleus affects the point where the compound nucleus will be formed.
Introducing a general transmission coefficient accounting for the creation of a compound nucleus with energy E spin J and parity π:

$$T(E,J,\pi) = \sum_{l=J-I_k}^{J+I_k} \sum_{I_i-I_j}^{I_i+I_j} T_{lI_k}(E) \quad (3)$$

we can now write Eq. 1 as:

$$\sigma(E) = \frac{\hbar^2\pi}{2\mu E} \frac{1+\delta_{ij}}{(2I_i+1)(2I_j+1)} \sum_{J,\pi} (2J+1)\, T(E,J,\pi) \quad (4)$$

Considering all the possible decay channels for the compound nucleus we can write the transmission coefficient for the outgoing particles T_m such that probability of a certain outgoing particle *m* can be given by:

$$P_m = \frac{T_m}{\sum_n T_n} \quad (5)$$

where *n* sums over all possible channels.

Assuming that the formation and the decay of the compound nucleus are independent events the cross section of the combined reactions is given by:

$$\sigma(E) = \frac{\hbar^2\pi}{2\mu E} \frac{1+\delta_{ij}}{(2I_i+1)(2I_j+1)} \sum_{J,\pi} (2J+1) \frac{T(E,J,\pi) T_m(E,J,\pi)}{T_{tot}(E,J,\pi)} \quad (6)$$

Eq. 6 is the Hauser-Feshbach formula or the statistical model formula.

RESULTS

We calculated (n, γ) reaction rates (RR) for all the experimentally known mass values reported in AME20. We calculated mass values within the experimental errors. To calculate the reaction rate of a nucleus ${}^{A}_{Z}X$ we use two sets of mass values. The first set will give the maximum reaction rate by allowing for the maximum Q-value within 1 σ error according to AME20. This can be achieved if assume for the mass (M):

$$\mathrm{M}\,({}^{A}_{Z}X) = \mathrm{M}\,({}^{A}_{Z}X) + \mathrm{M\_error}\,({}^{A}_{Z}X) \quad (7)$$

$$\mathrm{M}\,({}^{A+1}_{Z}X) = \mathrm{M}\,({}^{A+1}_{Z}X) - \mathrm{M\_error}\,({}^{A+1}_{Z}X) \quad (8)$$

The calculated RR corresponding to the maximum Q-value is denoted by RR_{max}.

Similarly, we can account for the minimum Q-value within 1 σ error according to AME20 by inversing the signs of Eq. 7 and Eq. 8. We denote the RR corresponding to the minimum Q-value as RR_{min}. We can then calculate a percentage difference (denoted as I_{index}) between RR_{max} and RR_{min} for each isotope such that:

$$I_{index} = \frac{|RR_{max} - RR_{min}|}{1/2(RR_{max} + RR_{min})}$$

We find that the calculated RR close to the last experimental known mass where the uncertainties are larger can differ by a factor of two or more (Fig. 4). In addition, we observe that mass-excess uncertainties of up to 20 keV do not have a strong impact on the calculation of reaction rates. These results agree with Fig. 3 where we see the uncertainties for the isotopes in the vicinity of ^{132}Sn. We note that the reaction rates that are affected the most are the last known isotope of each element. This

is because in order to determine the last known isotope with A we need to use the extrapolated mass value whith the associated with higher uncertainties of the neighboring isotope with A+1.

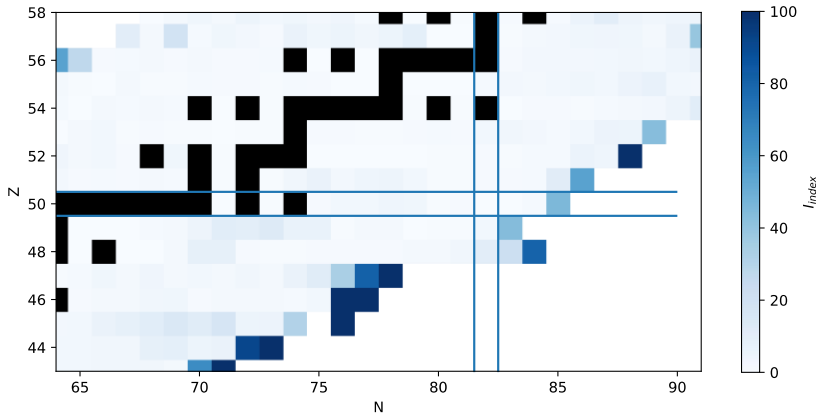

Fig. 4 *The reaction-rate difference index I_{index} shown on the neutron vs proton number plane (N-Z plane). With black squares we label stable nuclei. Vertical and horizontal lines label the N=82 closed neutron and Z=50 proton shell respectively.*

SUMMARY

We explored the isotopes in the vicinity of the ^{132}Sn, which is responsible for the formation of the first r-process peak. We stress the importance of new mass measurements with new experimental techniques for possible corrections of previous mass measurements or error reductions.

Acknowledgments

The authors want to acknowledge funding from the European Union's Horizon 2020 research and innovation programme (ERC Consolidator Grant 2017) under grant agreement No. 771036 project MAIDEN.

References

[1] E. M. Burbidge et al., Rev. Mod. Phys., vol. 29, no. 4, pp. 547–650, (1957)
[2] J. Cowan et al., Rev. Mod. Phys., vol. 93 pp. 015002, (2021)
[3] J. J. Cowan and C. Sneden, Nature, vol. 440, no. 7088, pp. 1151–1156, (2006)
[4] S. Nikas et al., HNPS Adv. in Nucl. Phys., vol. 27, pp. 175–179, (2020)
[5] M. R. Mumpower et al., Phys. Rev. C, vol. 86, no. 3, p. 35803, (2012)
[6] A. Aprahamian et al., AIP Advances, vol. 4, no. 4, p. 41101, (2014)
[7] M. R. Mumpower et al., Prog. in Part. and Nucl. Phys., vol. 86, pp. 86–126, (2016)
[8] C. Sneden and J. J. Cowan, Science, vol. 299, no. 5603, pp. 70–75, (2003)
[9] D. Kasen et al., Nature, vol. 551, no. 7678, pp. 80–84, (2017)
[10] C. Freiburghaus et al., AJ, vol. 525, no. 2, pp. (1999)
[11] D. Radice et al., MNRAS, vol. 460, no. 3, pp. 3255–3271, (2016)
[12] S. Goriely et al., AJL, vol. 738, no. 2, p. L32, (2011)
[13] M. Eichler et al., AJ, vol. 808, p. 30, Jul. (2015)
[14] M.-R. Wu et al., MNRAS, vol. 463, no. 3, pp. 2323–2334, (2016)
[15] M. R. Mumpower et al., Journal of Physics G vol. 44, p. 30, (2017)
[16] S. Goriely, A&A, vol. 342, pp. 881–891, (1999)
[17] M. R. Mumpower et al., EPJ Web Conf., (2014)
[18] S. Nikas, thesis Central Michigan University Library (2017)
[19] S. Nikas et al., arXiv preprint arXiv:2010.01698, (2020)
[20] M. Reiter et al. Phys. Rev. C, vol. 101 p. 025803, (2020)

[21] S. Eliseev et al., PRL, vol. 110, no. 8, p. 082501, (2013)
[22] T. Dickel et al., Hyper. Inter. vol. 240, pp. 1–9, (2019)
[23] M. Wang et al., Chin. Phys. C, vol. 41, no. 3, p. 30003, (2017)
[24] M. Wang et al., Chin. Phys. C, vol. 45, no. 3, p. 30003, (2021)
[25] A. Kankainen et al., Hyper. Inter. vol. 241, no. 1, pp. 1–14, (2020)
[26] A. J. Koning and D. Rochman, Nuc. data sheets, vol. 113, no. 12, pp. 2841–2934, (2012)
[27] P. Capel International Scientific Meeting on Nuclear Physics-Basic concepts in Nuclear Physics: theory, experiments, and applications, pp. 33–74, (2018)